RSC Advances

PAPER

View Article Online
View Journal | View Issue

Cite this: *RSC Adv.*, 2016, **6**, 937

A chitosan–Pt nanoparticles/carbon nanotubes-doped phosphomolybdate nanocomposite as a platform for the sensitive detection of nitrite in tap water†

Zhenyuan Bai, Chunlei Zhou, Ning Gao, Haijun Pang and Huiyuan Ma*

Received 20th September 2015
Accepted 28th November 2015

DOI: 10.1039/c5ra19383d

www.rsc.org/advances

A composite multilayer film was fabricated based on $H_7P_2Mo_{17}V_1O_{62}$ ($P_2Mo_{17}V$)–carbon nanotubes (CNTs) and Pt–chitosan (Pt–CHIT) nanoparticles using layer-by-layer self-assembly method. The incorporation of CNTs and Pt–CHIT nanoparticles into the $P_2Mo_{17}V$-based composite film endowed the modified electrode with a fast electron transfer rate and high electrocatalytic activity towards nitrite oxidation. The as-prepared sensor showed a fast response to nitrite with a good linear concentration range from 1.25×10^{-7} M to 4.167×10^{-3} M and a high sensitivity of 0.019 μA mM^{-1}. Most noteworthy is its ultra-low detection limit of 3.8×10^{-9} M at the signal-to-noise ratio of 3 under optimal experimental conditions, which was below the detection limit of the vast majority of nitrite sensors reported before. The as-prepared sensor was able to distinguish the oxidation response of common interferences in solution mixtures under multiple potentials. It was successfully applied for determination of nitrite in tap water samples with satisfactory results.

1. Introduction

Nitrite is a highly toxic substance, which widely exists among environmental, food and physiological systems, such as in tap water, food additives and soil.[1] As a hazardous substance, nitrite can react with dietary components to form toxic and carcinogenic nitrosamines in the stomach.[2,3] Thus, there are specific requirements concerning nitrite levels; the maximum permissible amount of nitrite ions in drinking water is 50 mg L^{-1} according to the World Health Organization.[2,4] Much concern has been shown about the level of nitrite in tap water, foods and beverages, and accurate determination of nitrite is essential to reduce the health risks. In recent years, many analytical techniques have been developed for the detection of nitrite, mainly involving spectrophotometry,[5] fluorescence,[6] flow injection analysis,[7] chromatography,[8] capillary electrophoresis chemiluminescence[9] and so on. However, using these methods demands tedious and time consuming sample pretreatment and expensive reagents. Therefore, it is desirable to develop simple and low cost methods to determine nitrite. Electrochemical techniques, which are characterized by their low cost, easy operation and high sensitivity, have aroused widespread interest.[10]

New assembly techniques are required for creating advanced materials with enough structural flexibility to be tuned for specific applications, and to be practical, the techniques must be implemented at relatively low cost.[11] Layer-by-layer (LBL) self-assembly is a ubiquitous phenomenon in nature at molecular and supramolecular levels, and it has been proven to be a promising and useful bottom-up approach to prepare functional materials. Compared with other available assembly methods, LBL is simplicity[12,13] and the controllability of the thickness, composition, morphology, structure and physicochemical properties.[14,15] To date, a variety of materials such as polyelectrolytes,[16,17] nanoparticles,[18–20] and inorganic materials[21,22] have been employed for the construction of LBL films. This versatility has led to recent exceptional growth in the use of LBL-generated nanocomposites and is becoming a very attractive and powerful technology for the development of sensors because this technique is simple, universal, low cost and environmentally-friendly.

Polyoxometalates (POMs), as one of the most important inorganic building blocks, not only possess rich structural versatility such as Keggin, Wells–Dawson, Lindqvist types, *etc.*, but also demonstrate superior redox activity.[23,24] POMs can undergo reversible multielectron redox transformations without any significant structural alteration under rather mild conditions, which makes them play an important role as catalysts.[25,26] In the recent study, polyoxotungstates and

Key Laboratory of Green Chemical Engineering and Technology of College of Heilongjiang Province, College of Chemical and Environmental Engineering, Harbin University of Science and Technology, Harbin 150040, China. E-mail: mahy017@163.com; Fax: +86-0451-86392716; Tel: +86-0451-86392716

† Electronic supplementary information (ESI) available: The characterization of Pt–CHIT nanoparticle and XPS spectra of the composite film, additional electrochemical investigations. See DOI: 10.1039/c5ra19383d

polyoxomolybdates have been extensively studied as electrocatalysts.[27,28] However, the electrochemical and electrocatalytic properties of the vanadium-substituted polyoxometalates have been studied much less than those of the parent polyanions. The substitution of Mo^{VI} (or W^{VI}) by V^{V} allows the adjustment of the electrochemical properties of POMs since the oxidizing ability decreases in the following order: $V^{V} > Mo^{VI} > W^{VI}$. Moreover, substitution of vanadium into the POM framework can shift the stability of the species to higher pH values, which is a key factor in several (electro)catalytic processes.[29–31] Meanwhile, the immobilization of POMs onto the variable electrode surface, while maintaining and enhancing their beneficial properties is important for their applications in areas of electrocatalyst and sensor.[32]

Multiwall carbon nanotubes (MWCNTs) with extraordinary mechanical strength, high surface to volume ratio, excellent electrical conductivity and high chemical stability[33–35] have received considerable attention in recent years including the fabrication of electrochemical sensors and elevation the sensitivity and electrocatalytic activity of the corresponding sensor devices.[36] Over the past few years, the investigation of POMs-modified CNTs has become a fascinating subject. Given the excellent structural and electronic properties of CNTs and POMs, the development of POMs-modified CNTs as electrode materials has attracted significant attention. Song *et al.* investigated the electrocatalytic properties of the composite film CNTs–SiW_{11}.[37] Chen *et al.* fabricated a composite film containing PMo_{12}-modified CNTs and Pt or Pt–Ru, and then they studied its electrochemical properties towards methanol electro-oxidation.[38] What's more, CNTs can not only serve as promising catalyst supports[39] but also can integrate with metal nanoparticles to form a composite with remarkable activity for small molecules.

The uses of noble metal nanoparticles have gained considerable attention because of their size-dependent electrical, chemical and optical properties.[40] We are interested in the catalytic and electrochemical properties of highly dispersed platinum nanoparticles. Polyelectrolyte chitosan (CHIT), as a typical biological macromolecule, possesses remarkable characteristics, such as excellent biodegradability, biocompatibility, and non-toxicity.[41,42] Therefore, it can be used as cationic polyelectrolyte for the formation of LBL films when its functions are protonated in acid solutions. Many applications of chitosan depend on the interaction between amino groups and anionic surface-active substances, such as small molecule surfactants, phospholipids, or polyoxometalate.[43] That is to say, the interaction between amino groups and anionic compounds can significantly enhance the stability of the immobilized system. So CHIT was chosen to simply produce stable Pt nanoparticles in this paper.

Based on the above description, this work focuses on fabrication of a composite film with high electrocatalytic activity for nitrite consisting of the Pt–CHIT NPs, $P_2Mo_{17}V$ and CNTs using layer-by-layer self-assembly method. The procedure involved in the preparation of this composite film is very flexible and highly reproducible. The film growth was monitored by UV-vis spectroscopy, surface morphology and topography was examined by atomic force microscopy (AFM), and composition was assessed by X-ray photoelectron spectroscopy (XPS). The sensing performance of the composite film for the detection of nitrite at phosphate buffer solution (pH = 6.0) was investigated by cyclic voltammetry and amperometric response. This novel sensor offers a very good selectivity and ultra-low detection limit of nitrite. Furthermore, it was successfully used to determine nitrite in tap water.

2. Experimental

2.1. Materials and apparatus

$H_7P_2Mo_{17}V_1O_{62}$ ($P_2Mo_{17}V$) was synthesized according to the literature method,[44] and then identified by FT-IR and cyclic voltammetry analysis. Poly(ethylenimine) (PEI MW 750 000) and poly(styrenesulfonate) (PSS MW 70 000) were commercially purchased from Aldrich and used without further purification. H_2PtCl_6 (MW 232) and chitosan (CHIT) were purchased from Sigma-Aldrich China Co. Ltd. All other reagents were analytical grade and prepared with deionized water (18 MΩ cm). Multi-walled carbon nanotubes (MWCNTs, with >95% purity, diameter 15–20 nm) were obtained from College of Materials and Chemistry and Chemistry Engineering, Heilongjiang University (Harbin, China).

AFM images were obtained by Dimension TM3100 series of AFM produced from Digital Instruments (Santa Barbara, California, USA). TEM images were obtained on an H-7650 TEM. UV-vis absorption spectra were recorded on a quartz slide using a U-3900 UV-vis spectrophotometer from Hitachi (Japan). Cyclic voltammetry (CV) was conducted by a CHI760D Electrochemical Workstation (Shanghai Chenhua Instrument Corporation, China), with a conventional three-electrode system in which the modified ITO or bare ITO electrode was used as the working electrode, an Ag/AgCl as the reference electrode and a platinum wire as counter electrode.

2.2. Substrate preparation

ITO-coated glass was cleaned by immersing it in a series of ultrasonically agitated solvents (30% KOH alcohol solution, ethanol, H_2O) at 40 °C for 20 min. A quartz or silicon substrate was immersed into fresh piranha solution (30% H_2O_2/98% H_2SO_4, v/v = 3 : 7; **CAUTION**: piranha solutions are very aggressive and corrosive; appropriate safety precautions should be utilized, including the use of acid-resistant gloves and adequate shielding.) and heated until no bubbles were released. The substrate was carefully rinsed with deionized water and dried with nitrogen. The substrates were then immersed in solution of PEI (0.1 mg mL^{-1}) for one night to form the self-assembled monolayer terminated with $-NH_2$ functional groups at the exposed surface. Subsequently, the quartz or silicon substrate was rinsed with deionized water and dried for further experiments. The amino units acted as the donor to construct the assembly by cooperating bonding.

2.3. Syntheses of the Pt–CHIT nanoparticles

According to the ref. 45, briefly, a 0.2 wt% CHIT solution was prepared by dissolving 40 mg of CHIT flakes into 10 mL of 1.0% acetic acid and stirred for 3 h at room temperature until

complete dissolution. The pH of resulting solution was adjusted to 3.0–4.0 using a concentrated NaOH solution, followed by the addition of 2 mL of 0.01 M H_2PtCl_6, and the solution was sonicated for 15 min. Then the Pt(IV) was reduced by using 1 mL of freshly prepared 5% $NaBH_4$. Reduction of $PtCl_6^-$ by $NaBH_4$ yields a clear yellow brown colored solution. The proposed Pt–CHIT nanoparticles were characterized by TEM (Fig. S1†), which are highly monodispersed with an average diameter of *ca.* 6 nm. The prepared Pt–CHIT solution has very excellent stability, and no aggregation of nanoparticles was noticed after four months when the solution was stored in the dark at room temperature.

2.4. Fabrication of the composite films

The {PEI/[$P_2Mo_{17}V$-PSS-CNTs/Pt–CHIT]$_n$/$P_2Mo_{17}V$-PSS-CNTs} multilayer films were assembled on different substrates due to their convenience for a particular analysis method: quartz slides for UV-vis spectroscopy, silicon wafers for AFM, and ITO-coated glass for XPS and cyclic voltammetry studies.

First, the PEI was deposited onto a cleaned substrate by immersing the substrate in PEI (10 mM) solutions for one night, in order to reduce possible interference from the substrate and to form a more uniformly charged surface,[46–48] followed by rinsing with deionized water and drying under a nitrogen stream. And then, the pre-coated substrate was alternately immersed in the $P_2Mo_{17}V$-PSS-CNTs suspension (3.0 mg mL^{-1} of $P_2Mo_{17}V$ mixed with 1.0 mg mL^{-1} PSS and 1.0 mg mL^{-1} of CNTs, w/w/w = 3 : 1 : 1) and Pt–CHIT aqueous solution for 30 min and rinsed with deionized water after each immersing. This procedure was repeated as many times as the number of bilayers needed, the composite film {PEI/[$P_2Mo_{17}V$-PSS-CNTs/Pt–CHIT]$_n$/$P_2Mo_{17}V$-PSS-CNTs} was formed. The whole preparation process of the composite film is shown in Scheme 1. For comparison, the films {PEI/[$P_2Mo_{17}V$/Pt–CHIT]$_n$/$P_2Mo_{17}V$}, {PEI/[PSS-CNTs/Pt–CHIT]$_n$} and {PEI/[$P_2Mo_{17}V$-PSS-CNTs/CHIT]$_n$/$P_2Mo_{17}V$-PSS-CNTs} were prepared according to the same procedure.

3. Results and discussion

3.1. {$P_2Mo_{17}V$-PSS-CNTs/Pt–CHIT}$_n$ film growth

UV-vis spectroscopy was used to monitor the layer-by-layer self-assembling process of the composite film owing to its facility in evaluating the growth process of the multilayers film. Fig. 1 depicts the UV-vis spectra of {PEI/[$P_2Mo_{17}V$-PSS-CNTs/Pt–CHIT]$_n$} films, with n = 1–10, in the range of 180–800 nm. The spectra showed three peaks at 194, 224, and 310 nm, respectively. As is reported, over our investigated wavelength range, Pt nanoparticles has one characteristic absorption at 195 nm,[49] $P_2Mo_{17}V$ has two characteristic absorptions in the polyoxometalate cage, Mo–O charge-transfer absorption at 226 nm and V–O charge-transfer absorption at 312 nm,[50] PSS has two characteristic absorptions of pendent aromatic groups at 195 and 225 nm.[51] So the absorption at 194 nm can be assigned to the overlap peak of Pt nanoparticles and PSS, the absorption at 224 nm can be assigned to the overlap peak of PSS and $P_2Mo_{17}V$, the absorption at 310 nm can be assigned to $P_2Mo_{17}V$. The absorbance in the wavelength range of 180–800 nm increases steadily with the bilayer number, which confirmed the irreversible adsorption of $P_2Mo_{17}V$-PSS-CNTs and Pt–CHIT on the composite film.

As the numbers of bilayers increased there was an linear increment in the absorbance at λ_{max} = 224 nm (the inset of Fig. 1), which this suggests that the amount of material deposited in each bilayer is constant and consistent with a stepwise growth process for this LBL hybrid film up to 10 layers. This is indicative of strong interaction between the

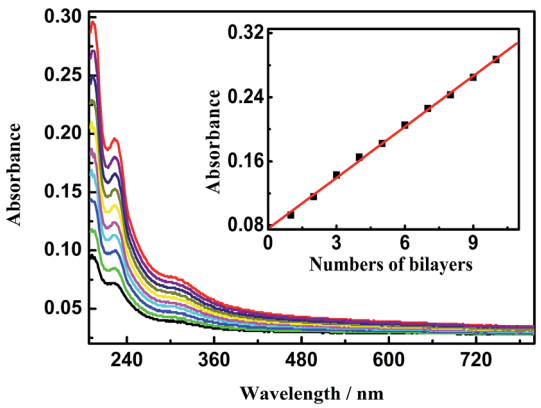

Fig. 1 UV-vis absorption spectra of the composite film {PEI/[$P_2Mo_{17}V$-PSS-CNTs/Pt–CHIT]$_n$/$P_2Mo_{17}V$-PSS-CNTs} for n = 1–10 adsorbed on a quartz slide. The inset shows the absorbance at λ_{max} = 224 nm as a function of n.

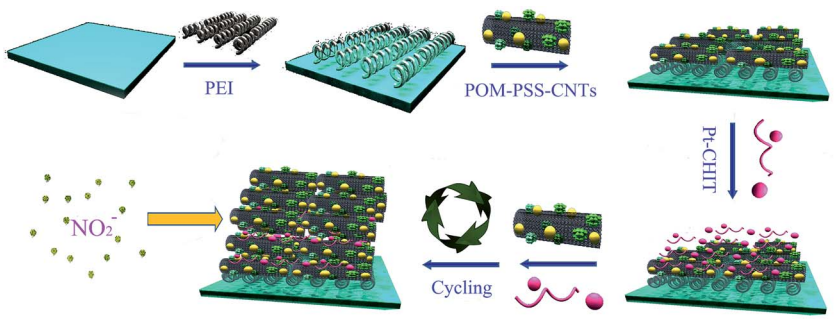

Scheme 1 Schematic illustration of the as-prepared sensor.

charged components $P_2Mo_{17}V$-PSS-CNTs and Pt–CHIT, each deposition cycle is uniform and stable. From the UV-vis spectra, the surface coverage (Γ) of $P_2Mo_{17}V$ can be calculated according to the following equation: $\Gamma = (N_A A_\lambda)/2m\varepsilon_\lambda$,[52–54] where N_A is Avogadro's constant, A_λ is the absorbance at a given wavelength λ (310 nm), ε_λ is the molar extinction coefficient ($\varepsilon_{310} = 1.036 \times 10^6$ M^{-1} cm^{-1}) and m (10) is the number of layer. The average surface coverage calculated from UV-vis spectra is *ca.* 5.724×10^{15} $P_2Mo_{17}V$ anions per cm^{-2} or 9.508×10^{-9} mol cm^{-2}.

3.2. Surface morphology

Tapping mode AFM image of the {PEI/[$P_2Mo_{17}V$-PSS-CNTs/Pt–CHIT]$_{10}$/$P_2Mo_{17}V$-PSS-CNTs} multilayer film was performed to find out its surface topography. Fig. 2 shows the AFM image of the composite film adsorbed on a silicon substrate.

From the typical three-dimensional AFM image of this composite film, it is clearly observed that the surface of the composite film was covered by a lot of protuberant peaks. The particle size and root-mean-square (RMS) roughness of the film is 85.9 and 6.34 nm calculated over an area of 10×10 μm^2. It was reported that the low roughness and vertical grain structure with gap are particularly suitable for the fabrication of large-area and thin-film electronic devices.[32]

The presence of elemental composition in the multilayer film of {PEI/[$P_2Mo_{17}V$-PSS-CNTs/Pt–CHIT]$_{10}$/$P_2Mo_{17}V$-PSS-CNTs} deposited on the silicon was verified by XPS, as indicated in Fig. S2.† The spectrum of Pt reveals doublet peaks of Pt $4f_{7/2}$ and Pt $4f_{5/2}$ levels at 73.4 and 75.1 eV, respectively, which is identical to platinum in the zero-valent state in the film.[55,56] From the Fig. S2(b)–(d),† one peak of P 2p at 133.1 eV, two peaks of Mo 3d at 232.6 and 235.8 eV, and one V 2p peak at 533 eV were observed.[28,57] Furthermore, the spectrum of C 1s (Fig. S2(e)†) shows two peaks at approximately 284.5 and 286.1 eV. The peak at 284.5 eV is attributed to the aliphatic carbon (–C–C– or –C–H–), and that at 286.1 eV is attributed to carbon bonded to the amine groups (–C–NR_2, where R is C or H) of the chitosan. The N 1s spectrum (Fig. S2(f)†) displays double peaks at 399.3 and 401.5 eV, which are corresponding to amine and amide, respectively.[58,59] These results substantiated that $P_2Mo_{17}V$, carbon nanotube and Pt–CHIT NPs were indeed incorporated into the composite film, which were consistent with UV spectra.

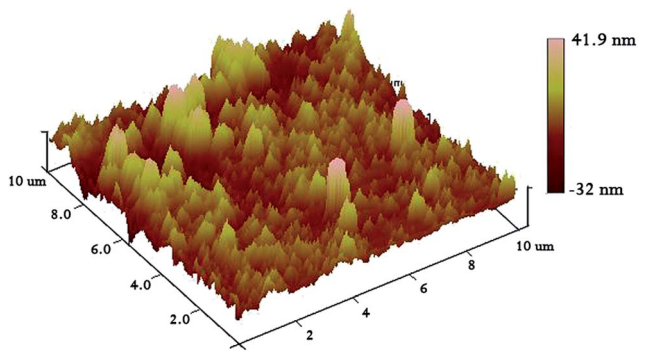

Fig. 2 Tapping mode 3D AFM image of {PEI/[$P_2Mo_{17}V$-PSS-CNTs/Pt–CHIT]$_{10}$/$P_2Mo_{17}V$-PSS-CNTs} deposited on a silicon wafer.

3.3. Electrochemical characterization of composite films

The CVs of the composite film {PEI/[$P_2Mo_{17}V$-PSS-CNTs/Pt–CHIT]$_{10}$/$P_2Mo_{17}V$-PSS-CNTs} at different scan rates are shown in Fig. 3. It can be seen that when the scan rate increased from 100 to 800 mV s^{-1}, the cathodic peak currents and the corresponding anodic peak currents increased simultaneously. The composite film {PEI/[$P_2Mo_{17}V$-PSS-CNTs/Pt–CHIT]$_{10}$/$P_2Mo_{17}V$-PSS-CNTs} shows three pairs of strong redox peaks with mean peak potentials $E_{1/2}$ of −0.579 V, −0.406 V and −0.249 V, and two pairs of very weak redox peaks with mean peak potentials $E_{1/2}$ of −0.016 V, 0.558 V respectively *vs.* Ag/AgCl attributed to the immobilized $P_2Mo_{17}V$. In this context, the pair I is corresponding to one-electron of vanadium-center ($V^V \rightarrow V^{IV}$), II and III correspond to two one-electron Mo-centered reduction processes ($Mo^{VI} \rightarrow Mo^V$),[31] while the other two peaks (IV and V) correspond to two two-electron Mo-centered ($Mo^{VI} \rightarrow Mo^V$).[60] From the inset of Fig. 3, we can see the dependence of the cathodic and anodic peak currents of the forth pair wave on scan rates, which is indicative of a surface confined electrochemical process.

Electrochemical surface coverage (Γ) of electroactive species immobilized at electrode surfaces can be estimated from cyclic voltammetry according to the equation $\Gamma = (4i_pRT)/(n^2F^2\nu A)$, where i_p is the peak current (amperes), n is the number of electrons transferred, ν is the scan rate (V s^{-1}), A is the geometric area of the working electrode (square centimeters), R is the gas constant, T is the temperature (298 K), and F is Faraday's constant.[61] The surface coverage of $P_2Mo_{17}V$ can be directly calculated from the peak current i_p because the polyelectrolyte matrix is not electroactive in the whole experiment. Taking the forth couple of redox peaks as example, the surface coverage of $P_2Mo_{17}V$ per layer amounts to 1.66×10^{-8} mol cm^{-2} for the composite film {PEI/{[$P_2Mo_{17}V$-PSS-CNTs/Pt–CHIT]$_{10}$/$P_2Mo_{17}V$-PSS-CNTs} at scan rate of 0.1 V s^{-1}. This result is in agreement with the surface coverage of 9.508×10^{-9} mol cm^{-2} determined by UV-vis spectra.

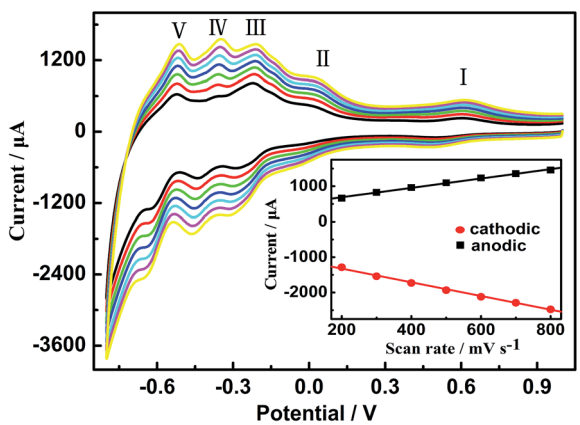

Fig. 3 Cyclic voltammograms of the composite film {PEI/[$P_2Mo_{17}V$-PSS-CNTs/Pt–CHIT]$_{10}$ $P_2Mo_{17}V$-PSS-CNTs } in 0.2 M PBS (pH = 6.0) *vs.* Ag/AgCl at different scan rates (from inner to outer: 100, 200, 300, 400, 500, 600, 700 and 800 mV s^{-1}). The inset: plots of the cathodic and anodic peak currents of the fifth couple waves against scan rate.

3.4. Electrochemical impedance spectra

The complex impedance can be presented as the sum of the real (Z_{re}) and imaginary (Z_{im}) components that originate mainly from the resistance and capacitance of the films. The semicircle diameter of EIS equals the electron transfer resistance (R_{et}), which controls the electron transfer kinetics of the redox probe at the electrode interface. In this work, R_{et} reflects the restricted diffusion of the redox probe through the multilayer system, which relates directly to the accessibility of the underlying electrode.[62,63] The EIS figures of the {PEI/[$P_2Mo_{17}V$-PSS-CNTs/Pt–CHIT]$_{10}$/$P_2Mo_{17}V$-PSS-CNTs}, {PEI/[CNTs-PSS/Pt–CHIT]$_{10}$}, {PEI[$P_2Mo_{17}V$/Pt–CHIT]$_{10}$/$P_2Mo_{17}V$} and {PEI/[$P_2Mo_{17}V$-PSS-CNTs/CHIT]$_{10}$/$P_2Mo_{17}V$-PSS-CNTs} films are shown in Fig. 4. The frequency range was between 0.01 and 1 000 000 Hz with signal amplitude of 5 mV. The diameter of the semicircle increases in the order of the {PEI/[$P_2Mo_{17}V$-PSS-CNTs/Pt–CHIT]$_{10}$/$P_2Mo_{17}V$-PSS-CNTs} < {PEI/[CNTs-PSS/Pt–CHIT]$_{10}$} < {PEI[$P_2Mo_{17}V$/Pt–CHIT]$_{10}$/$P_2Mo_{17}V$} < {PEI/[$P_2Mo_{17}V$-PSS-CNTs/CHIT]$_{10}$/$P_2Mo_{17}V$-PSS-CNTs} < bare ITO. This result indicates a lower electron transfer resistance and larger electron transfer rate in the composite film {PEI/[$P_2Mo_{17}V$-PSS-CNTs/Pt–CHIT]$_{10}$/$P_2Mo_{17}V$-PSS-CNTs}. That is to say, the synergy between $P_2Mo_{17}V$-PSS-CNTs and Pt–CHIT could accelerate the electron transfer in the composite film. The electrode system can be simplified by a equivalent circuit, and the inset of Fig. 4 shows a equivalent circuit obtained from the obtained impedance data of the composite film {PEI/[$P_2Mo_{17}V$-PSS-CNTs/Pt–CHIT]$_{10}$/$P_2Mo_{17}V$-PSS-CNTs}. The equivalent circuit included the following parameters: R_s is the ohmic resistance of the electrolyte solution; R_p is the resistance to charge transfer. In this simple equivalent circuit, it was assumed that the resistance to charge transfer (R_p) was in parallel to the constant phase element (CPE), which was selected to replace the pure capacitor in the equivalent circuit by considering the surface roughness and inhomogeneity of the composite film. This parallel combination of R_p and CPE1 gave rise to a semicircle in the complex plane plot of Z_{im} against Z_{re}. According to the result of impedance spectrum, R_p was 1275 Ω and CPE was 8.0812 × 10^{-5} F. The electric charge transmission speed constant (k) can be calculated by the following formula:[64,65] $k = RT/R_pCn^2F^2A$, where R_p is the resistance to charge transfer, n is the number of electrons transferred per electroactive specie, C is the constant phase element (CPE), A is the geometric area of the electrode (square centimeters), and all other terms have their usual meaning. According to the formula, the electric charge transmission speed constant (k_0) of the composite film {PEI/[$P_2Mo_{17}V$-PSS-CNTs/Pt–CHIT]$_{10}$/$P_2Mo_{17}V$-PSS-CNTs} was estimated to be 1.72 × 10^{-6} cm s^{-1}, while the electric charge transmission speed constant (k) of bare ITO, the {PEI/[$P_2Mo_{17}V$-PSS-CNTs/CHIT]$_{10}$/$P_2Mo_{17}V$-PSS-CNTs}, the {PEI[$P_2Mo_{17}V$/Pt–CHIT]$_{10}$/$P_2Mo_{17}V$} and {PEI/[CNTs-PSS/Pt–CHIT]$_{10}$} films were estimated to be 9.81 × 10^{-11} cm s^{-1}, 6.64 × 10^{-9} cm s^{-1}, 1.84 × 10^{-9} cm s^{-1} and 4.67 × 10^{-7} cm s^{-1}, respectively. From the above results, it is clearly noted that the incorporation the CNTs, $P_2Mo_{17}V$ and Pt–CHIT nanoparticle could improve the conductivity of the composite film.

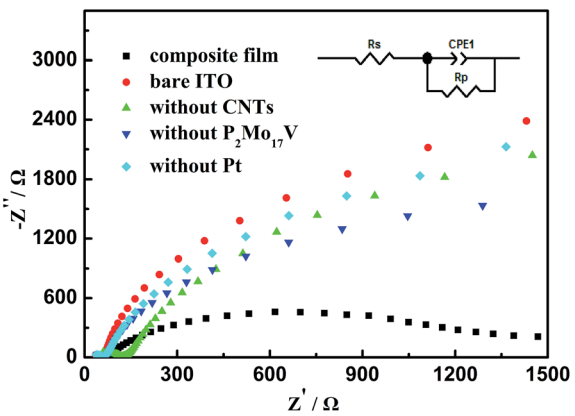

Fig. 4 The EIS figure of the composite film {PEI/[$P_2Mo_{17}V$-PSS-CNTs/Pt–CHIT]$_{10}$/$P_2Mo_{17}V$-PSS-CNTs} (black dot), film {PEI/[CNTs-PSS/Pt–CHIT]$_{10}$} (dark blue dot), {PEI/[$P_2Mo_{17}V$/Pt–CHIT]$_{10}$/$P_2Mo_{17}V$} (green dot), {PEI/[$P_2Mo_{17}V$-PSS-CNTs/CHIT]$_{10}$/$P_2Mo_{17}V$-PSS-CNTs} (light blue dot) and bare ITO (red dot) in 0.2 M PBS (pH = 6.0), the inset: a simple equivalent circuit about the composite film electrode.

3.5. Electrocatalytic studies

The electroactive LBL films usually can enhance the reduction/oxidation of many species by acting as mediators between the substrate and the bare electrode. In this work, the prepared {PEI/[$P_2Mo_{17}V$-PSS-CNTs/Pt–CHIT]$_n$/$P_2Mo_{17}V$-PSS-CNTs} multilayer film was used as working electrode to improve the oxidation of nitrite to build a high sensitive sensor of nitrite.

A series of comparative experiments for the {PEI/[$P_2Mo_{17}V$-PSS-CNTs/Pt–CHIT]$_n$/$P_2Mo_{17}V$-PSS-CNTs} film were performed to the oxidation of nitrite to seek the optimized bilayer number and pH. The parallel electrocatalytic experiments of the composite film {PEI/[$P_2Mo_{17}V$-PSS-CNTs/Pt–CHIT]$_n$/$P_2Mo_{17}V$-PSS-CNTs} with different bilayer numbers (n = 2, 4, 6, 8, 10, 12 and 14) towards oxidation of nitrite were performed. The electrocatalytic activity of POM toward oxidation of nitrite can be evaluated by calculating the electrocatalytic efficiency (CAT) using the equation below:[66]

$$\mathrm{CAT} = 100\% \times [i_p(\mathrm{POMs}, NO_2^-) - i_p(\mathrm{POMs})]/i_p(\mathrm{POMs})$$

where i_p(POMs) and i_p(POMs, NO_2^-) are the catalytic currents of the POMs in the absence and presence of NO_2^-, respectively. When 0.3 mM nitrite was added, the electrocatalytic efficiencies of the composite film {PEI/[$P_2Mo_{17}V$-PSS-CNTs/Pt–CHIT]$_n$/$P_2Mo_{17}V$-PSS-CNTs} with different bilayer numbers (n = 2, 4, 6, 8, 10, 12 and 14) are 210%, 478%, 372%, 286%, 961%, 156% and 169%, respectively (see Fig. S3(a)†). It can be seen that 10-bilayer composite film has the highest catalytic efficiency, the reason of the 12 and 14 bilayer composite films having lower catalytic efficiency probably is that electron transport and reactant mass transport become limiting in thicker films.[67] Meanwhile, the oxidation of nitrite by the {PEI/[$P_2Mo_{17}V$-PSS-CNTs/Pt–CHIT]$_{10}$/$P_2Mo_{17}V$-PSS-CNTs} composite film in different pH solutions ranging from 5.0 to 7.0 was carried out. As shown in Fig. S3(b),† the pH has a large effect on the electrocatalytic efficiencies, and

the electrocatalytic efficiencies of the {PEI/[$P_2Mo_{17}V$-PSS-CNTs/Pt–CHIT]$_{10}$/$P_2Mo_{17}V$-PSS-CNTs} composite film toward oxidation of nitrite is the largest (961%) in pH = 6.0 phosphate buffer solution. So, to give the as-prepared sensor with higher catalytic efficiency, 10-bilayers composite film was chosen as the working electrode and pH = 6.0 phosphate buffer solution as the buffer solution in follow experiments.

Fig. 5 shows the CVs obtained from the {PEI/[$P_2Mo_{17}V$-PSS-CNTs/Pt–CHIT]$_{10}$/$P_2Mo_{17}V$-PSS-CNTs} composite film in the absence and in the presence of increasing concentrations of nitrite in the interval from 0.1 to 0.5 mM, which recorded in the potential range of 0.3 V to 1.0 V at scan rate 50 mV s^{-1}. It can be seen that the anodic peak current at about +0.9 V of the composite film gradually increased with the addition of NO_2^-, which indicates an electrocatalytic effect in the electrooxidation of NO_2^-. The inset of Fig. 5 shows the relationship between the concentrations of NO_2^- and catalytic currents. From the inset, it can be seen that with the increase of the concentrations of NO_2^-, the corresponding catalytic currents of the anodic peak enhanced linearly, which indicates different concentrations of NO_2^- can be quantified. The analysis of the corresponding current intensities leads to CAT = 961% for the electrooxidation of nitrite (3×10^{-4} mol dm^{-3}). In comparison, oxidation of NO_2^- by three different composite films {PEI/[CNTs-PSS/Pt–CHIT]$_{10}$}, {PEI/[$P_2Mo_{17}V$/Pt–CHIT]$_{10}$/$P_2Mo_{17}V$} and {PEI/[$P_2Mo_{17}V$-PSS-CNTs/CHIT]$_{10}$/$P_2Mo_{17}V$-PSS-CNTs} were investigated respectively. When 0.3 mM NO_2^- is catalyzed, the catalytic efficiency of the film {PEI/[CNTs-PSS/Pt–CHIT]$_{10}$} is 510%, the film {PEI/[$P_2Mo_{17}V$/Pt–CHIT]$_{10}$/$P_2Mo_{17}V$} is 110%, and that of the film {PEI/[$P_2Mo_{17}V$-PSS-CNTs/CHIT]$_{10}$/$P_2Mo_{17}V$-PSS-CNTs} is 154% (calculated from Fig. S4(a)–(c),† respectively), which are significantly lower than that of the composite film {PEI/[$P_2Mo_{17}V$-PSS-CNTs/Pt–CHIT]$_{10}$/$P_2Mo_{17}V$-PSS-CNTs} (961%). The high CAT indicated that this composite film offers a significant electrocatalysis of nitrite.

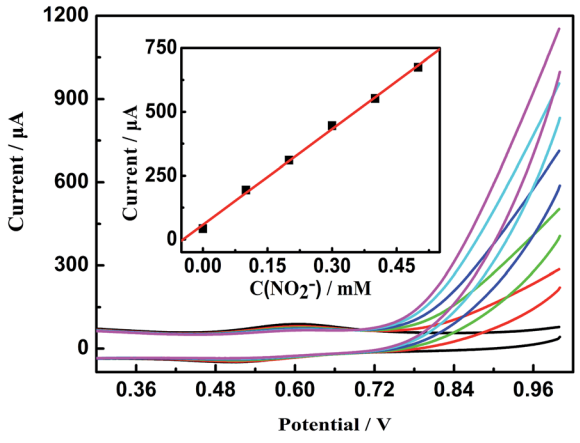

Fig. 5 Cyclic voltammograms of the composite film {PEI/[$P_2Mo_{17}V$-PSS-CNTs/Pt–CHIT]$_{10}$/$P_2Mo_{17}V$-PSS-CNTs} in 0.2 M PBS (pH = 6.0) obtained with different concentrations of NO_2^-: (0, 0.1, 0.2, 0.3, 0.4 and 0.5 mM); scan rate 50 mV s^{-1}. The inset shows the catalytic peak current *vs.* analyte concentration at 0.9 V.

The significant enhancement in the catalytic efficiency of the composite film {PEI/[$P_2Mo_{17}V$-PSS-CNTs/Pt–CHIT]$_{10}$/$P_2Mo_{17}V$-PSS-CNTs} may be arising from the change of the electron transport pathway in the composite film ascribed to the combination of the electroactive CNTs, $P_2Mo_{17}V$ and Pt–CHIT in the composite film. Polyoxometalate acts as a proton and electron reservoir in the electrocatalytic process, and the good electrical conductivity and large surface area of the CNTs and Pt–CHIT nanoparticles facilitate the electron transfer and provide active sites. And the coexistence of CNTs, Pt–CHIT and $P_2Mo_{17}V^VO_{62}^{7-}$ improve significantly the kinetics process of nitrite oxidation. Chitosan group nanoparticles have more advantages than normal nanoparticles, since they are allowed to fabricate more permeable films. As a result, remarkable catalytic efficiency enhancement of the composite film electrode was observed. That is to say, the incorporation of CNTs into the V-substituted POM and introduction the Pt nanoparticles into CHIT solution could constitute a useful strategy for the preparation of electrochemical sensors with improved sensing performance.

In the neutral conditions (PBS, pH = 6.0), the nitrite is oxidized to nitrate according to the following reaction:[68]

$$NO_2^- + H_2O \rightarrow NO_3^- + 2H^+ + 2e^-$$

The vanadium is the reactive site for this catalytic reaction.[10] The NO_2^- is oxidized by $P_2Mo_{17}V^VO_{62}^{7-}$ to yield NO_3^- and the one-electron reduced species $P_2Mo_{17}V^{IV}O_{62}^{7-}$.

3.6. Analytical evaluation of the nitrite sensor

3.6.1. Amperometric detection of the NO_2^-. Under optimal conditions, amperometric responses upon successive addition of NO_2^- were detected on {PEI/[$P_2Mo_{17}V$-PSS-CNTs/Pt–CHIT]$_{10}$/$P_2Mo_{17}V$-PSS-CNTs} in 0.2 M PBS (pH = 6.0) at +0.9 V through 1200 s at 50 s interval. The typical amperometric response curves of different concentrations of NO_2^- are shown in Fig. 6(a). A well-defined, stable and fast amperometric response increasing step-wise with the level of NO_2^- can be observed, demonstrating highly efficient catalytic ability of composite film for NO_2^- electrooxidation. The response time (defined as the time to achieve 95% steady-state current) of this as-prepared sensor was estimated to be 2 s from the inset of Fig. 6(a), which is far less than what has been achieved by Malika Ammam (<6 s),[69] Malcolm R. Smyth (5 s)[70] and Pei-Hui Yang (5 s),[71] and is some less than that achieved by Shan-Shan Li (3 s).[2] As a potential candidate for routine nitrite analysis in tap water, improving the response time is very necessary. The current responses are linear with NO_2^- concentrations from 1.25×10^{-7} to 4.167×10^{-3} M, with the regression equation as: $I_{NO_2^-}$ (μA) = 0.435 + 0.019$C_{NO_2^-}$ (mM), R^2 = 0.99809 (see Fig. 6(b)). The limit of detection assessed as 3 × S/*D* is estimated to be 3.8×10^{-9} M (S/N = 3) and the sensitivity is 0.019 μA mM^{-1}. As we know, many NO_2^- sensors have been developed by using POMs or other materials. A comparison of the performance of our newly as-prepared sensor with those already reported in literatures regarding the performance of the NO_2^- assay was listed in

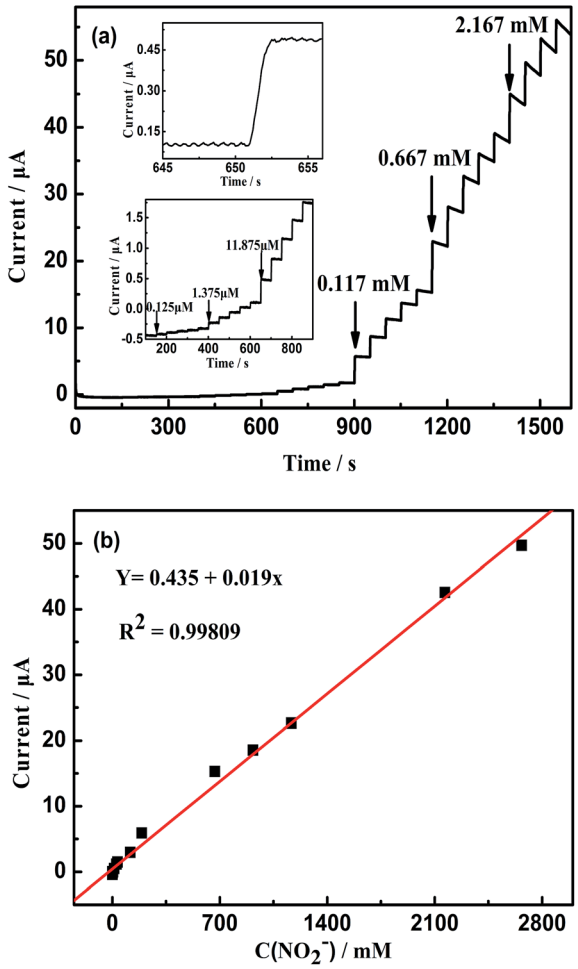

Fig. 6 (a) Typical amperometric responses curve of the composite film {PEI/[P_2Mo_{17}V-PSS-CNTs/Pt–CHIT]$_{10}$/P_2Mo_{17}V-PSS-CNTs} to successive additions of NO_2^- at applied potential of 0.9 V *vs.* Ag/AgCl in 0.2 M PBS (pH = 6.0). The insets show the enlargement of parts of curve. (b) Calibration plot of steady-state currents obtained at the composite film {PEI/[P_2Mo_{17}V-PSS-CNTs/Pt–CHIT]$_{10}$/P_2Mo_{17}V-PSS-CNTs} against concentrations of NO_2^-.

Table 1. It can be seen from Table 1 that this sensor has competitive performance among these sensors. Specially, linear response range and detection limit of this as-prepared sensor are superior to those sensors reported before. These results indicated that this as-prepared nitrite sensor could be an excellent platform for the detection of nitrite.

3.6.2. Sensitivity and selectivity. It is well-known that the sensitivity and selectivity of the electrochemical sensors are markedly dependent on the applied potential. In order to determine whether this sensor is affected by the presence of common interferent in food system, the possible interference for the detection of NO_2^- at the as-prepared electrode was investigated by adding various foreign chemical species into the solution, including C_2H_5OH, acetic acid, phosphoric acid, glucose, Na_2SO_4, $KBrO_3$, citric acid, Na_2CO_3, KCl and KNO_3. From Fig. 7, it can be obtained that catalytic current of NO_2^- oxidation by the composite film {PEI/[P_2Mo_{17}V-PSS-CNTs/Pt–CHIT]$_{10}$/P_2Mo_{17}V-PSS-CNTs} increased with the positive shift of the applied potential, showing the sensitivity of this sensor is dependent on the applied potential, and the more positive the applied potential is the higher sensitivity of this sensor shows. On the other hand, it can be concluded that at all applied potentials the interferences of these ten species toward this electrochemical sensor is nearly negligible, demonstrating that this as-prepared sensor has very superior selectivity. It was also noted that at the applied potentials of +0.9 and +1.0 V, the sensitivity of the sensor is superior and suitable, but in order to

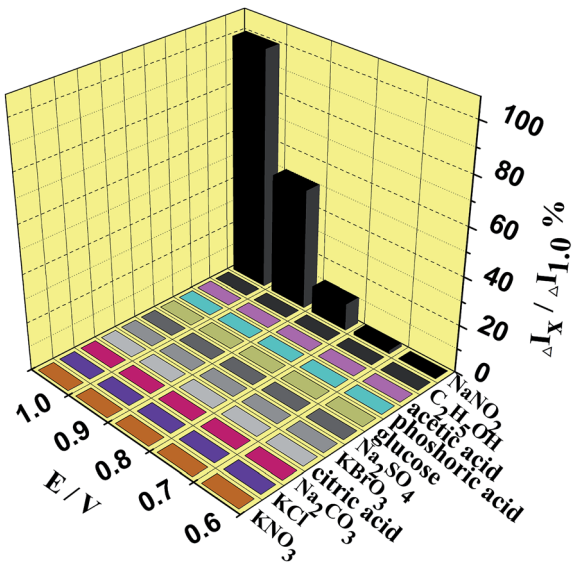

Fig. 7 The selectivity profile of the composite film obtained with 0.5 mM NO_2^-, C_2H_5OH, acetic acid, phosphoric acid, glucose, Na_2SO_4, $KBrO_3$, citric acid, Na_2CO_3, KCl and KNO_3 at different applied potentials 0.6, 0.7, 0.8, 0.9 and 1.0 V in 0.2 M PBS (pH = 6.0).

Table 1 Comparative characteristics of this as-prepared sensor and some other sensors for the determination of nitrite

Electrode	Method	Working potential (V)	Linear range (mol L^{-1})	LOD (μM)	Ref.
$K_6[P_2W_{18}O_{62}]$/ITO	CV	−0.22	1.0×10^{-4} to 1.5×10^{-3}	0.96	72
$POMs(PFS\text{-}POMs)_4$/cysteamine/Au	CV	−0.07	2.0×10^{-5} to 2.0×10^{-2}	1.56	73
PDDA/P_2W_{17}V–CNTs/ITO	CV	0.9	0.05×10^{-6} to 2.13×10^{-3}	0.0367	10
CDP–GS–MWCNTs	CV	0.7	5×10^{-6} to 6.75×10^{-3}	1.65	74
Au–RGO/PDDA	DPV	0.89	0.05×10^{-6} to 8.5×10^{-3}	0.04	75
La–MWCNTs/GCE	CA	0.75	0.4×10^{-6} to 0.71×10^{-3}	0.13	76
P_2Mo_{17}V-PSS-CNTs/Pt–CHIT/ITO	CV	0.9	1.25×10^{-7} to 4.167×10^{-3}	0.0038	This work

give this as-prepared sensor lower energy consumption, +0.9 V (*vs.* Ag/AgCl) is chosen as the optimized applied potential for determination of NO_2^-.

3.6.3. Reproducibility and stability. The reproducibility and stability of the proposed nitrite sensor were further evaluated. As shown in Fig. 8, the stability of the sensor was checked by cyclic voltammetry scanning for 100 cycles from −0.6 V to 1.2 V at 50 mV s^{-1} in 0.2 M PBS (pH = 6.0), which testifies the good stability of the as-prepared sensor. In order to study the reproducibility of the sensor, the catalytic efficiency of ten identically modified electrodes in 0.2 M PBS which contained 0.3 mM NO_2^- were investigated under the same experimental conditions (see Table S1 and Fig. S5†). According to the Table S1 and Fig. S5,† the relative standard deviation (RSD) can be calculated to be only 3.56% by the following formula: RSD = SD/$\bar{x}$, which demonstrated excellent reproducibility. Good reproducibility and high stability of the as-prepared sensor make it possible for durable and reliable sensing nitrite in practical application.

3.7. Nitrite sample analysis

In order to verify the practicality of the proposed sensor, it was applied to detect nitrite in real sample (tap water). Typically, added 4 mL real sample into the stirring solution containing 40 mL, 0.2 M PBS (pH = 6.0). Then the standard nitrite (0.01 mol L^{-1}) solution was added into above mentioned solution six times to accomplish the detection. By standard addition method (see Fig. S6†), a linear relation was obtained for the catalytic current I (μA) *versus* NO_2^- concentration C (mM) ($I = -3.212 + 226.278 \times C$, $R^2 = 0.997$). The concentration of NO_2^- can be obtained from the above-mentioned linear regression equation and then the recovery was calculated (see Table 2), all these results indicated that the proposed sensor could be used for the direct detection of nitrite in real sample with a good average recovery of 100.83%.

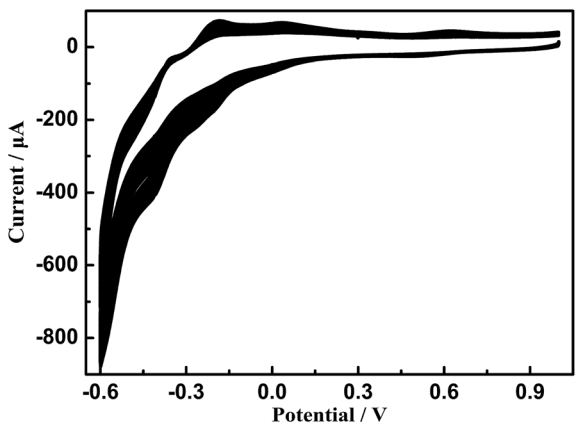

Fig. 8 Cyclic voltammograms of the composite film {PEI/[$P_2Mo_{17}V$-PSS-CNTs/Pt–CHIT]$_{10}$/$P_2Mo_{17}V$-PSS-CNTs} curves for 100 cycles in 0.2 M PBS (pH = 6.0). Scan rate: 50 mV s^{-1}.

Table 2 Results of the determination of nitrite in different samples[a]

Sample	NO_2^- added (mM)	NO_2^- found (mM)	Recovery (%)
1	0.02273	0.0305	134.18
2	0.06818	0.07356	107.89
3	0.1136	0.11662	102.66
4	0.1591	0.15968	100.36
5	0.2273	0.22428	98.67
6	0.2727	0.26734	98.03
7	0.3409	0.33193	97.37

[a] The average recovery (%) was 100.83%.

4. Conclusions

In summary, a composite film for sensing nitrite was fabricated by incorporating Dawson-type polyoxometalate $P_2Mo_{17}V$, CNTs and Pt–CHIT NPs using LBL self-assembly method. By integrating $P_2Mo_{17}V$, CNTs and Pt–CHIT NPs into the composite film, the synergistic effect among all components was realized and maximized, leading to superior performance in electrocatalysis compared to any component alone. The significant advantages of this novel composite film include: (1) unique 3-D structure of CNTs facilitated high loading of active $P_2Mo_{17}V$ and Pt–CHIT NPs on to the electrode surface and enhanced the electrocatalysis efficiency for nitrite. (2) CNTs maximized the dispersion of Pt–CHIT and $P_2Mo_{17}V$, and increased robustness of the whole composite film. (3) High electrical conductivity and active surface area of CNTs and Pt–CHIT NPs relieved the surface fouling effect, and enhanced the electron transfer rate between the molecules and electrode. Compared to other pre-reported nitrite sensors, this sensor possesses wide liner range, ultra-low detection limit, excellent selectivity, and highly reproducible as well as easy fabrication. It could be used practically in tap water. This investigation provided a methodology to promote the development of highly sensitive, selective, and durable and reproducible composite electrodes to be used in electrochemical sensor devices.

Acknowledgements

This work was financially supported by the NSF of China (21371041, 51572063), the science and technology innovation foundation of Harbin (2014RFXXJ076).

References

1 X. Li, C. T. Wei, Y. H. Song, H. Z. Zhu, S. H. Chen, P. Li, L. L. Sun and L. Wang, *Environ. Eng. Sci.*, 2015, **32**, 185.
2 S. S. Li, Y. Y. Hu, A. J. Wang, X. X. Weng, J. R. Chen and J. J. Feng, *Sens. Actuators, B*, 2015, **208**, 468.
3 Y. L. Zhao, D. A. Zhao and D. L. Li, *Int. J. Electrochem. Sci.*, 2015, **10**, 1144.
4 J. Y. Qu, Y. Dong, Y. Wang and H. H. Xing, *Sens. Biosensing Res.*, 2015, **3**, 74.
5 V. Vishnuvardhan, R. Kala and T. P. Rao, *Anal. Chim. Acta*, 2008, **623**, 53.
6 C. C. Ju, H. J. Yin, C. L. Yuan and K. Z. Wang, *Spectrochim. Acta, Part A*, 2011, **79**, 1876.

7 M. Yaqoob, B. F. Biot, A. Nabi and P. J. Worsfold, *Luminescence*, 2012, **27**, 419.
8 I. M. P. L. V. O. Ferreira and S. Silva, *Talanta*, 2008, **74**, 1598.
9 H. X. Zhang, L. J. Zhang, C. Lu, L. X. Zhao and Z. X. Zheng, *Spectrochim. Acta, Part A*, 2012, **85**, 217.
10 D. Zhang, H. Y. Ma, Y. Y. Chen, H. J. Pang and Y. Yu, *Anal. Chim. Acta*, 2013, **792**, 35.
11 S. Srivastava and N. A. Kotov, *Acc. Chem. Res.*, 2008, **41**, 1831.
12 G. Decher, M. Eckle, J. Schmitt and B. Struth, *Curr. Opin. Colloid Interface Sci.*, 1998, **3**, 32.
13 S. T. Dubas and J. B. Schlenoff, *Macromolecules*, 1999, **32**, 8153.
14 N. Ferreyra, L. C. Guérente, J. Fatisson, M. L. Teijelo and P. Labbé, *Chem. Commun.*, 2003, 2056.
15 F. X. Zhang and M. P. Srinivasan, *Langmuir*, 2007, **23**, 10102.
16 N. Anwar, M. Vagin, R. Naseer, S. Imar, M. Ibrahim, S. S. Mal, U. Kortz, F. Laffir and T. McCormac, *Langmuir*, 2012, **28**, 5480.
17 H. Paloniemi, M. Lukkarinen, T. Ääritalo, S. Areva, J. Leiro, M. Heinonen, K. Haapakka and J. Lukkari, *Langmuir*, 2006, **22**, 74.
18 A. Devadoss, J. W. Lee, C. Terashima, A. Fujishima, Y. P. Kim, J. K. Kang and U. Paik, *Sens. Actuators, B*, 2015, **208**, 204.
19 J. P. Wang, H. Gao, F. L. Sun and C. X. Xu, *Sens. Actuators, B*, 2014, **191**, 612.
20 M. Li, X. J. Bo, Z. C. Mu, Y. F. Zhang and L. P. Guo, *Sens. Actuators, B*, 2014, **192**, 261.
21 D. M. Fernandes, C. M. A. Brett and A. M. V. Cavaleiro, *J. Solid State Electrochem.*, 2011, **15**, 811.
22 S. Q. Liu and Z. Y. Tang, *Nano Today*, 2010, **5**, 267.
23 S. Khadempir, A. Ahmadpour, M. T. H. Mosavian, N. Ashraf, F. F. Bamoharram, S. G. Mitchell and J. M. de la Fuente, *RSC Adv.*, 2015, **5**, 24319.
24 M. Vasilopoulou, A. M. Douvas, L. C. Palilis, S. Kennou and P. Argitis, *J. Am. Chem. Soc.*, 2015, **137**, 6844.
25 D. Y. Du, J. S. Qin, S. L. Li, Z. M. Su and Y. Q. Lan, *Chem. Soc. Rev.*, 2014, **43**, 4615.
26 S. Herrmann, C. Ritchie and C. Streb, *Dalton Trans.*, 2015, **44**, 7092.
27 D. Zhang, Y. Y. Chen, H. J. Pang, Y. Yu and H. Y. Ma, *Electrochim. Acta*, 2013, **105**, 560.
28 D. M. Fernandes, A. Teixeira and C. Freire, *Langmuir*, 2015, **31**, 1855.
29 M. Sadakane and E. Steckhan, *Chem. Rev.*, 1998, **98**, 219.
30 P. Mialane, J. Marrot, E. Rivière, J. Nebout and G. Hervé, *Inorg. Chem.*, 2001, **40**, 44.
31 D. M. Fernandes, A. D. S. Barbosa, J. Pires, S. S. Balula, L. C. Silva and C. Freire, *ACS Appl. Mater. Interfaces*, 2013, **5**, 13382.
32 C. L. Zhou, S. Li, W. Zhu, H. J. Pang and H. Y. Ma, *Electrochim. Acta*, 2013, **113**, 454.
33 X. L. Xia, D. W. Fan, B. H. An, Y. Y. Cai and Q. Wei, *J. Mol. Liq.*, 2015, **206**, 335.
34 E. T. Thostenson, Z. F. Ren and T. W. Chou, *Compos. Sci. Technol.*, 2001, **61**, 1899.
35 N. Butwong, L. Zhou, W. Ng-eontae, R. Burakham, E. Moore, S. Srijaranai, J. H. T. Luong and J. D. Glennon, *J. Electroanal. Chem.*, 2014, **717–718**, 41.
36 M. M. Barsan, M. E. Ghica and C. M. A. Brett, *Anal. Chim. Acta*, 2015, **881**, 1.
37 W. Chen, L. J. Huang, J. Hu, T. F. Li, F. F. Jia and Y. F. Song, *Phys. Chem. Chem. Phys.*, 2014, **16**, 19668.
38 D. W. Pan, J. H. Chen, W. Y. Tao, L. H. Nie and S. Z. Yao, *Langmuir*, 2006, **22**, 5872.
39 K. Mukhopadhyay, S. Phadtare, V. P. Vinod, A. Kumar, M. Rao, R. V. Chaudhari and M. Sastry, *Langmuir*, 2003, **19**, 3858.
40 C. L. Tan, X. Huang and H. Zhang, *Mater. Today*, 2013, **16**, 29.
41 P. Sorlier, A. Denuzière, C. Viton and A. Domard, *Biomacromolecules*, 2001, **2**, 765.
42 M. Rinaudo, *Prog. Polym. Sci.*, 2006, **31**, 603.
43 B. Krajewska, *Enzyme Microb. Technol.*, 2004, **35**, 126.
44 D. R. Park, H. Kim, J. C. Jung, S. H. Lee and I. K. Song, *Catal. Commun.*, 2008, **9**, 293.
45 M. H. Yang, Y. Yang, H. F. Yang, G. L. Shen and R. Q. Yu, *Biomaterials*, 2006, **27**, 246.
46 C. Q. Peng, Y. S. Thio and R. A. Gerhardt, *Langmuir*, 2012, **28**, 84.
47 D. Lee, Z. Gemici, M. F. Rubner and R. E. Cohen, *Langmuir*, 2007, **23**, 8833.
48 J. Bravo, L. Zhai, Z. Z. Wu, R. E. Cohen and M. F. Rubner, *Langmuir*, 2007, **23**, 7293.
49 S. Li, H. Y. Ma, K. P. O'Halloran, H. J. Pang, H. R. Ji and C. L. Zhou, *Electrochim. Acta*, 2013, **108**, 717.
50 H. Y. Ma, Y. Gu, Z. J. Zhang, H. J. Pang, S. Li and L. Kang, *Electrochim. Acta*, 2011, **56**, 7428.
51 H. Y. Ma, J. Peng, Y. H. Chen, Y. H. Feng and E. B. Wang, *J. Solid State Chem.*, 2004, **177**, 3333.
52 C. X. Li, K. P. O'Halloran, H. Y. Ma and S. L. Shi, *J. Phys. Chem. B*, 2009, **113**, 8043.
53 I. Creaser, M. C. Heckel, R. J. Neitz and M. T. Pope, *Inorg. Chem.*, 1993, **32**, 1573.
54 F. Caruso, D. G. Kurth, D. Volkmer, M. J. Koop and A. Müller, *Langmuir*, 1998, **14**, 3462.
55 Z. J. Mei, Y. Li, M. H. Fan, L. Zhao and J. Zhao, *Chem. Eng. J.*, 2015, **259**, 293.
56 X. Zhang, X. J. Zan and Z. H. Su, *J. Mater. Chem.*, 2011, **21**, 17783.
57 Y. Y. Bao, L. H. Bin and L. X. Wu, *J. Solid State Chem.*, 2011, **184**, 546.
58 G. Lawrie, I. Keen, B. Drew, A. C. Temple, L. Rintoul, P. Fredericks and L. Grøndahl, *Biomacromolecules*, 2007, **8**, 2533.
59 L. Ning, W. J. Zhang, H. Yan, H. J. Pang, H. Y. Ma and Y. Yu, *J. Colloid Interface Sci.*, 2013, **403**, 91.
60 H. M. Ji, L. D. Zhu, D. D. Liang, Y. Liu, L. L. Cai, S. W. Zhang and S. X. Liu, *Electrochim. Acta*, 2009, **54**, 7429.
61 D. M. Fernandes and C. Freire, *J. Appl. Electrochem.*, 2014, **44**, 655.
62 S. Y. Gao, Z. X. Wu, D. M. Pan, Z. Lin and R. Cao, *Thin Solid Films*, 2011, **519**, 2317.

63 M. F. Shao, X. Y. Xu, J. B. Han, J. W. Zhao, W. Y. Shi, X. G. Kong, M. Wei, D. G. Evans and X. Duan, *Langmuir*, 2011, **27**, 8233.
64 E. Sabatani and I. Rubinstein, *J. Phys. Chem.*, 1987, **91**, 6663.
65 L. Chen, L. Tian, L. Liu, X. F. Tian, W. B. Song, H. D. Xu and X. H. Wang, *Sens. Actuators, B*, 2005, **110**, 271.
66 D. M. Fernandes, J. G. Vos and C. Freire, *J. Colloid Interface Sci.*, 2014, **420**, 127.
67 C. J. Campbell, C. K. Njue, B. Nuthakki and J. F. Rusling, *Langmuir*, 2001, **17**, 3447.
68 W. L. Sun, F. Yang, H. Z. Liu, J. L. Kong, S. L. Jin, G. Y. Xie and J. Q. Deng, *J. Electroanal. Chem.*, 1998, **451**, 49.
69 M. Ammam, B. Keita, L. Nadjo and J. Fransaer, *Talanta*, 2010, **80**, 2140.
70 X. L. Luo, A. J. Killard and M. R. Smyth, *Chem.–Eur. J.*, 2007, **13**, 2143.
71 H. Wang, P. H. Yang, H. H. Cai and J. Y. Cai, *Synth. Met.*, 2012, **162**, 331.
72 F. Cao, S. Guo, H. Ma and J. Gong, *Electroanalysis*, 2012, **24**, 418.
73 C. Chen, Y. Song and L. Wang, *Electroanalysis*, 2008, **20**, 2543.
74 Y. Zhang, R. Yuan, Y. Q. Chai, W. J. Li, X. Zhong and H. A. Zhong, *Biosens. Bioelectron.*, 2011, **26**, 3977.
75 S. F. Jiao, J. Jin and L. Wang, *Sens. Actuators, B*, 2015, **208**, 36.
76 W. Zhang, R. Yuan, Y. Q. Chai, Y. Zhang and S. H. Chen, *Sens. Actuators, B*, 2012, **166–167**, 601.